JCTC Journal of Chemical Theory and Computation

Bulk and Surface Properties of Rutile TiO_2 from Self-Consistent-Charge Density Functional Tight Binding

H. Fox,[†] K. E. Newman,[‡] W. F. Schneider,[§] and S. A. Corcelli*,[†]

Department of Chemistry and Biochemistry, Department of Physics, Department of Chemical and Biomolecular Engineering, and Department of Chemistry and Biochemistry, University of Notre Dame, Notre Dame, Indiana 46556

Received October 2, 2009

Abstract: Bulk rutile TiO_2 and its (110) surface have been investigated with a computationally efficient semiempirical tight binding method: self-consistent-charge density functional tight binding (SCC-DFTB). Comparisons of energetic, mechanical, and electronic properties are made to density functional theory (DFT) and to experiment to characterize the accuracy of SCC-DFTB for bulk rutile TiO_2 and TiO_2(110). Despite the fact that the SCC-DFTB parameters for Ti, Ti−Ti, and Ti−O were developed in the context of small biologically relevant Ti containing compounds, SCC-DFTB predicts many properties of bulk TiO_2 and the TiO_2(110) surface with accuracy similar to local and gradient-corrected DFT. In particular, SCC-DFTB predicts a direct band gap of TiO_2 of 2.46 eV, which is in better agreement with experiment, 3.06 eV, than DFT utilizing the local density approximation (LDA), 2.0 eV. SCC-DFTB also performs similar in terms of accuracy as LDA-DFT for the phonon frequencies of the bulk lattice and for the relaxed geometry of the TiO_2(110) surface. SCC-DFTB does, however, overestimate the surface energy of TiO_2(110) compared to LDA-DFT. Nevertheless, the overall accuracy of SCC-DFTB, which is substantially more computationally efficient than DFT, is encouraging for bulk rutile TiO_2 and TiO_2(110).

I. Introduction

Self-consistent-charge density functional tight binding (SCC-DFTB) is a powerful semiempirical tight binding method, which retains much of the physics of density functional theory (DFT) at a significantly reduced computational cost.[1−5] SCC-DFTB utilizes an optimized linear combination of atomic orbitals basis set and attains its computational efficiency in part by precomputing and tabulating all of the necessary one- and two-center matrix elements and overlap integrals. Charge transfer and polarizability are introduced by allowing fluctuations in individual atomic charge densities.The reduced computational cost of SCC-DFTB relative to plane-wave DFT offers the opportunity to investigate the properties of complex interfaces that are inaccessible with other methods (e.g., catalysis at solid−liquid boundaries). Like any emerging computational methodology, it is important that its accuracy be fully evaluated before proceeding to more complex applications. Previous studies have successfully utilized SCC-DFTB to study materials[5] including zinc oxide and sulfide[6] and silicon dioxide and carbide[7,8] and the interaction of graphite surfaces with water,[9] as well as biological systems,[10−25] protonated water clusters,[26] and liquid water.[27]

SCC-DFTB has not, however, been fully evaluated for titania (TiO_2). Two previous studies have used DFTB (without the SCC correction) to investigate the electronic properties of TiO_2 nanostructures.[28,29] While these studies illustrated the breadth of applicability of DFTB, neither addressed properties of bulk TiO_2 nor was their focus on validation of the DFTB methodology. A more recent study by Luschtinetz et al. used SCC-DFTB to investigate the adsorption of phosphonic acid on the (101) surface of anatase TiO_2 and the (110) of rutile TiO_2.[30] These authors reported structural properties of bulk rutile TiO_2 and TiO_2(110)

* To whom correspondence should be addressed. E-mail: scorcell@nd.edu.

[†] Department of Chemistry and Biochemistry.

[‡] Department of Physics.

[§] Department of Chemical and Biomolecular Engineering and Department of Chemistry and Biochemistry.

10.1021/ct900665a
Published on Web 01/22/2010

predicted with SCC-DFTB, including lattice parameters of bulk rutile TiO_2 and atomic displacements normal to the optimized TiO_2(110) surface. This paper aims to provide a more comprehensive characterization of SCC-DFTB for bulk rutile TiO_2 and TiO_2(110) by considering a much more expansive set of properties, including the electronic band structures and vibrational properties of the materials. Also, in this paper we demonstrate that publicly available[31] SCC-DFTB parameters developed and evaluated for titanium atoms in biological contexts[32] are transferable to bulk rutile TiO_2 and the TiO_2(110) surface. This is important because it establishes the broad applicability of SCC-DFTB for Ti-containing compounds and materials without recourse to reparameterization for each new problem.

Titanium dioxide is thought of as a prototypical metal oxide and has been extensively studied experimentally and theoretically due to its many industrial applications, principally as a white pigment and in heterogeneous catalysis. Titania and zirconia (ZrO_2) are unique among transition metal oxides because they are stable in aqueous solution and are thus particularly important for aqueous radiation and photochemistry. For example, TiO_2 is a model system for the photocatalytic disproportionation of water into hydrogen and oxygen gases using solar light.[33−43] The dearth in our understanding of the factors that influence the thermodynamics, kinetics, and mechanisms of chemical reactions at liquid−solid interfaces presents a fundamental impediment to the rational design of improved low-temperature catalysts. Accurate computer simulations of reactivity at liquid−solid interfaces would offer tremendous insight and guidance for improvement of these systems, and due to the large number of atoms involved in such a calculation, an alternative to density functional theory that could capture the science at less computational cost would be very beneficial.

A review by Diebold provides a broad introduction to the physical and chemical properties of bulk TiO_2 and its surfaces.[44] The (110) surface is the most stable rutile surface, and its structure has been the focus of numerous theoretical and computational investigations. The energetics and structure of the rutile TiO_2(110) surface have been investigated with DFT using various plane-wave[45−47] and atomic orbital[48−50] implementations. Experimentally, a recent low-energy electron diffraction study by Lindsay et al.[51] has found good agreement with theoretical studies of the (110) surface, compared to the surface X-ray diffraction study by Charlton et al.[52] We will show in this paper that titanium dioxide is described well by SCC-DFTB relative to DFT results using the local density approximation (LDA)[53] or generalized gradient approximation (GGA).[54,55] We will first give a brief introduction to the SCC-DFTB method in section II; section III includes calculations of bulk rutile TiO_2 structural, electronic and vibrational properties; section IV repeats this for the (110) surface; and finally, concluding remarks are found in section V.

II. SCC-DFTB Methodology

There are a number of features of the DFTB method (without the SCC correction) that are responsible for its computational efficiency and transferability. Most central to the latter is that the total energy of the system is expressed within a tight-binding (TB) formalism, where the matrix elements are precomputed and tabulated:[3,10]

$$E^{\mathrm{DFTB}} = \sum_i \sum_{\mu\nu} c_\mu^i c_\nu^i H_{\mu\nu}^{(0)} + E_{\mathrm{rep}} \tag{1}$$

The sum i is over occupied Kohn−Sham orbitals, $\Psi^i(\mathbf{r})$, which have been expanded as a linear combination of atomic orbitals (LCAO) in a basis of confined local pseudoatomic orbitals for the valence electrons, $\phi_\nu(\mathbf{r} - \mathbf{R}_\alpha)$

$$\Psi^i(\mathbf{r}) = \sum_\nu c_\nu^i \phi_\nu(\mathbf{r} - \mathbf{R}_\alpha) \tag{2}$$

where c_ν^i are expansion coefficients, $\mathbf{r}$ is the position of the electron, and $\mathbf{R}_\alpha$ is the position of nucleus α. The local atomic orbitals are specific to each atom type and are determined by performing a DFT calculation on the isolated atom with an extra electrostatic potential term that confines the electron density to regions that are close to the nucleus, $(r/r_0)^M$. This confining potential contains two parameters, r_0 and M, that could in principle be optimized. However, in practice $M = 2$ and $r_0 \approx 2r_{\mathrm{cov}}$, where r_{cov} is the covalent radius of the atom, are found to be reasonable.

By invoking a two-center approximation, the nonzero Hamiltonian matrix elements, $H_{\mu\nu}^{(0)}$, appearing in eq 1 can be conveniently expressed as

$$H_{\mu\nu}^{(0)} = \begin{cases} \varepsilon_\mu^{\text{neutral free atom}} & \alpha = \beta \\ \langle \phi_\mu^\alpha | \hat{T} + \hat{V}_0^\alpha + \hat{V}_0^\beta | \phi_\nu^\beta \rangle & \alpha \neq \beta \end{cases} \tag{3}$$

where $\hat{T}$ is the single-electron kinetic energy operator, $\varepsilon_\mu^{\text{neutral free atom}}$ are the Kohn−Sham orbital eigenvalues of the neutral free atom, and the additional superscripts, α and β, denote orbitals on atomic sites. $\hat{V}_0^\alpha$ is the effective one-electron Kohn−Sham potential for the compressed reference density on atom α. $\hat{V}_0^\alpha$ is evaluated without the confining potential $(r/r_0)^M$ but using the self-consistently determined confined reference density on atom α. Precomputing and tabulating these matrix elements as a function of the interatomic separation, $R_{\alpha\beta} = |\mathbf{R}_\alpha - \mathbf{R}_\beta|$, results in a significant computational savings.

By applying the variational principle to eq 1, a set of algebraic equations is obtained

$$\sum_\nu c_\nu^i (H_{\mu\nu}^{(0)} - \varepsilon_i S_{\mu\nu}) = 0 \tag{4}$$

whose solution provides the Kohn−Sham orbital coefficients, c_ν^i, and eigenvalues, ε_i. In eq 4, $S_{\mu\nu} = \langle \phi_\mu | \phi_\nu \rangle$ represents the overlap between local pseudoatomic orbitals. Once the coefficients c_ν^i have been determined, the total energy of the system can be evaluated using eq 1, where E_{rep} denotes the total core−core repulsion energy. E_{rep} is calculated from short-ranged purely repulsive pair-potentials, $V_{\mathrm{rep}}(R_{\alpha\beta})$, as follows:

$$E_{\mathrm{rep}} = \sum_\alpha \sum_{\beta>\alpha} V_{\mathrm{rep}}(R_{\alpha\beta}) \tag{5}$$

The effective pair-potentials, $V_{rep}(R_{\alpha\beta})$, are obtained by empirically fitting E^{DFTB} to the corresponding total energy, E^{DFT}, computed with DFT for a set of configurations of an appropriately chosen reference system. Determining $V_{rep}(R_{\alpha\beta})$ empirically has both advantages and disadvantages. From a theoretical perspective, it makes the DFTB method not entirely ab initio and, in principle, less transferable. However, the empiricism improves the accuracy of DFTB by incorporating information from higher-level DFT calculations, and from a practical perspective, the DFTB method has proven itself as an accurate and computationally efficient alternative to self-consistent DFT calculations.

An exciting advantage of the DFTB formalism is that it can be systematically improved by incorporating the effects of charge transfer (i.e., electronic polarizability); the effects of charge transfer are especially important for the description of bonding between atoms of different polarity and the electronic structure of metal oxides. In the self-consistent-charge (SCC) extension of DFTB, the matrix elements in eq 3 are rigorously corrected (through second order in perturbation theory) to take into account small fluctuations in the atomic charge density[3,56]

$$E^{(2)} = \frac{1}{2}\sum_{\alpha}\sum_{\beta}\Delta q_{\alpha}\Delta q_{\beta}\gamma_{\alpha\beta} \tag{6}$$

where the $\Delta q_{\alpha} = q_{\alpha} - q_{\alpha}^{(0)}$ are atomic charge fluctuations. $\gamma_{\alpha\beta} = \gamma_{\alpha\beta}(U_{\alpha},U_{\beta},R_{\alpha\beta})$ is a function that has been derived analytically by Elstner et al.[3] to arrive at the fairly simple, but approximate, expression (using atomic units)

$$\gamma_{\alpha\beta} = \frac{1}{R_{\alpha\beta}} - f(\tau_{\alpha},\tau_{\beta},R_{\alpha\beta}) \tag{7}$$

where $f(\tau_{\alpha},\tau_{\beta},R_{\alpha\beta})$ is an exponentially decaying short-ranged function, and $\tau_{\alpha} = 16/5U_{\alpha}$ is given in terms of the Hubbard parameter for atom α, U_{α}. Physically, U_{α} is approximately twice the chemical hardness of the atom and can be readily computed by calculating the derivative of the highest occupied atomic orbital with respect to its occupation number using DFT.

Although the accuracy of the DFTB method is significantly increased by incorporating the role of charge transfer, the method becomes more computationally expensive because the atomic charges in eq 6 must be determined self-consistently. However, since the charges do not vary significantly between molecular dynamics time steps, few iterations are typically needed to achieve convergence. Furthermore, since all of the terms in the Hamiltonian matrix elements are still precomputed and tabulated, the SCC-DFTB method remains computationally efficient. Several recent papers have proposed further extension of the DFTB method by incorporating higher-order fluctuations in the charge density.[10,57]

SCC-DFTB calculations were performed using the program DFTB+.[58] All precomputed matrix elements are held in Slater−Koster files, downloaded from http://www.dftb.org. The mio parameter set was used for O−O interactions[3] and the trans3d parameter set for Ti−O, Ti−Ti interactions.[32]

III. Bulk Rutile TiO_2

A. Crystal Geometry and Bulk Modulus. The unit cell of titanium dioxide is tetragonal, with six atoms per unit cell. The geometry of the unit cell is described in terms of two lattice parameters, a and c, in addition to the internal parameter u. Using SCC-DFTB we calculated the equilibrium lattice parameters to be $a = 4.70$ Å and $c = 2.92$ Å and the internal parameter to be $u = 0.300$ Å, in agreement to within 3% of the experimental values of $a = 4.58$ Å, $c = 2.95$ Å, and $u = 0.305$ Å[59] and other theoretical calculations.[60] Our results for the equilibrium lattice parameters are also consistent with the results of Luschtinetz et al.[30] ($a = 4.61$ Å, $c = 2.97$ Å, and $u = 0.302$ Å) using different SCC-DFTB parameters for bulk rutile TiO_2. The calculated rutile structure is stable to symmetry-breaking distortions. SCC-DFTB predicts that the titanium and oxygen atoms have atomic charges of $0.814e$ and $-0.407e$, respectively. The bulk modulus, K, of the material was found by varying the volume of the unit cell and taking the second derivative of the energy U:

$$K = V\left.\frac{\partial^2 U}{\partial V^2}\right|_0 \tag{8}$$

where the subscript zero denotes that the derivatives are to be evaluated at the equilibrium cell geometry. SCC-DFTB yielded a bulk modulus of 243 GPa, compared to an experimental value of 210 GPa.[59] DFT calculations predict a bulk modulus in slightly better agreement with experiment. With the LDA functional the bulk modulus is overestimated (230 GPa), whereas with the PBE[54] functional it is underestimated (194 GPa).[60]

B. Electronic Structure. Titanium dioxide is a wide-band gap semiconductor with relatively strong ionicity, being of advantage in photoassisted dissociation of molecules. The chemical bonding is governed by the interaction between oxygen 2p and titanium 3d states, compared to other common semiconductors such as ZnO and GaAs. Figure 1 shows the band structure and density of states of TiO_2 calculated using SCC-DFTB, where the zero of energy has been taken as the top of the valence band. The band structure was obtained by self-consistently converging charges with a tolerance of 1×10^{-5} on a $4 \times 4 \times 8$ Monkhorst−Pack mesh[61] in **k**-space. These charges were then utilized in a nonself-consistent-charge calculation of the energy along the high-symmetry directions of the Brillouin zone. The lower valence bands, of mostly O 2s character, and upper valence bands, from hybridization between O 2p and Ti 3d states, compare qualitatively well with LDA-DFT[62] and PBE-DFT[63] results; however both the upper and lower valence band widths are underestimated. Table 1 compares numerical properties of the SCC-DFTB bulk rutile TiO_2 electronic structure with experiment and with DFT calculations using the LDA and PBE functionals. A direct band gap of 2.46 eV is predicted by SCC-DFTB, which agrees better with the experimental[64,65] value of 3.06 eV than LDA-DFT (2.0 eV)[62] and PBE-DFT (1.88 eV).[63] It should be noted that the LDA-DFT and PBE-DFT band structure calculations were performed using different basis sets. The biggest difference between the SCC-

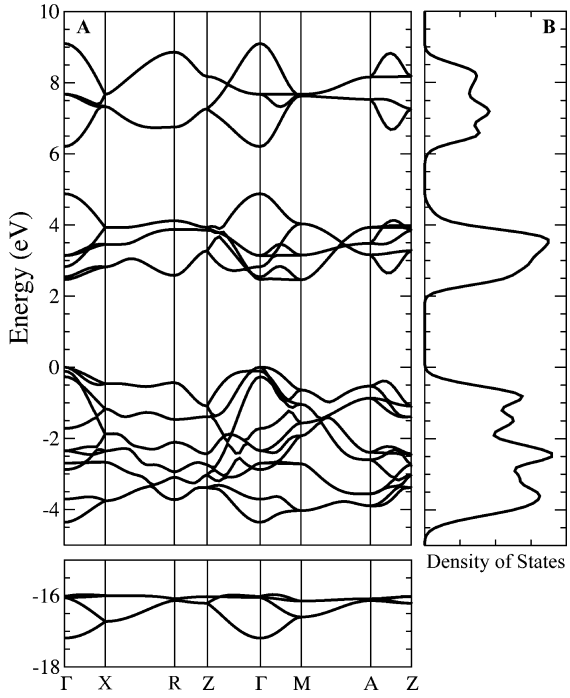

Figure 1. (A) Electronic band structure along high-symmetry directions of the irreducible Brillouin zone (Γ−X−R−Z−Γ−M−A−Z). For an illustration of the Brillouin zone of TiO_2, see, for example, Glassford and Chelikowsky.[62] (B) Electronic density of states.

Table 1. Electronic Structure of Bulk Rutile TiO_2

property	SCC-DFTB	PBE-DFT[a]	LDA-DFT[b]	experiment
lower valence bandwidth (eV)	1.22	1.79	1.8	1.9[c]
upper valence bandwidth (eV)	4.36	5.69	5.7	5.4[c]
lower valence/conduction band separation at Γ (eV)	18.5	18.13	17	16 − 18[d]
band gap (eV)	2.46	1.88	2.0	3.06[c,e]

[a] Reference 63. [b] Reference 62. [c] Reference 64. [d] Reference 86. [e] Reference 65.

DFTB and LDA-DFT band structures is in the conduction bands, where there is a gap of 1.2 eV at around 5 eV. The LDA-DFT results do find that the lower conduction bands can be divided into two distinct groups, corresponding to t_{2g} and e_g d orbital states of Ti, which are separated over the entire Brillouin zone, except for a small overlap at Γ. This overlap is absent in the SCC-DFTB band structure and is also absent in other empirical tight-binding studies.[66]

C. Vibrational Spectra. The lattice dynamics of bulk rutile titanium dioxide have been shown to be very important in determining its technological properties. For example, it has an exceptionally high static dielectric constant along the *c*-direction, which increases as the temperature is lowered. This has been explained in terms of the transverse optic A_{2u} mode, which is only 173 cm^{-1} at room temperature and shifts 36 cm^{-1} to the red at lower temperatures (142 cm^{-1} at 4 K).[67] This softness is not observed in isostructural materials like tin dioxide or germanium dioxide (465 and 455 cm^{-1}, respectively).

We calculated the vibrational frequencies of bulk titania at the Γ point using, first, the dynamical matrix method, where the frequencies are equal to the eigenvalues of the matrix D_{ij} defined by

$$D_{ij} = \frac{-1}{\sqrt{m_i m_j}} \left.\frac{\partial F_j}{\partial x_i}\right|_0 = \frac{1}{\sqrt{m_i m_j}} \left.\frac{\partial^2 E}{\partial x_i \partial x_j}\right|_0 \quad (9)$$

where m_i is the mass of atom i, x_i is the displacement of atom i from its equilibrium position, and the 0 subscript denotes that the derivatives are to be performed with all atoms in their equilibrium positions. D_{ij} is a $3N \times 3N$ matrix, where N here is 6, corresponding to the six atoms in the unit cell, and the eigenvectors of the matrix correspond to the displacements of the unit cell atoms in each of the various vibrational modes. The positions of the atoms in the unit cell were optimized until all forces were less than 10^{-4} eV/Å, and then a displacement of 0.01 Å was made in each of the $3N$ degrees of freedom. The derivative of the force was then calculated using a finite difference approximation. Second, we computed vibrational frequencies of selected modes using the frozen phonon method, which models a single mode directly and extracts a frequency from the energy found as a function of displacement. This method can readily expose any instabilities or anharmonicity, but it requires knowledge of the symmetry and displacement vector of a nondegenerate mode of interest. In contrast, the dynamical matrix method does not require any a priori information regarding the vibrational modes. When computing vibrational frequencies with the frozen phonon method, we used three displacements of 0.01 Å in the positive and negative directions to map the potential energy (−0.03, −0.02, −0.01, 0.00, 0.01, 0.02, 0.03 Å), which was then fit to a quadratic form to obtain the vibrational frequency of the mode.

Shown in Table 2 are bulk rutile TiO_2 vibrational frequencies computed with SCC-DFTB using both the dynamical matrix and the frozen phonon methods (frozen phonon frequencies were computed for four selected modes: B_{2g}, A_{1g}, E_g, and A_{2u}). For comparison we also show vibrational frequencies measured with several experimental techniques, including neutron scattering,[67] Raman scattering,[68] and infrared absorption.[69] Table 2 also contains bulk rutile TiO_2 vibrational frequencies reported by Sikora for LDA-DFT,[70] which are consistent and therefore representative of earlier DFT calculations,[60,71] and PBE-DFT results reported by Montanari and Harrison.[60] Four modes (A_{2u}, E_u^1, E_u^2, and E_u^3) that are strongly perturbed by an interaction with the electric fields created by long wavelength vibrations of the crystal [i.e., modes that undergo longitudinal optical-transverse optical (LO-TO) splitting] are omitted from Table 2. Correcting for LO-TO splitting to make a meaningful comparison to experiment requires a more sophisticated analysis and is inconsequential to validating the accuracy of SCC-DFTB for TiO_2. The agreement with experiment of the SCC-DFTB vibrational frequencies is generally impressive. For the higher frequency modes (>400 cm^{-1}) the root-mean-squared (rms) deviation of the calculated frequencies compared to the neutron scattering measurements is slightly better for SCC-DFTB than for LDA-DFT and PBE-DFT (16.4 cm^{-1} compared to 17.1 and 39.3 cm^{-1}). The lower frequency modes are significantly more challenging to compute correctly. For example, PBE-DFT predicts that the A_{2u} mode

Table 2. Calculated and Measured Bulk TiO_2 Phonon Frequencies (in cm^{-1})

	SCC-DFTB					
mode	dynamical matrix	frozen phonon	neutron scattering[67]	IR[69] and Raman[68]	PBE-DFT[60]	LDA-DFT[70]
B_{2g}	822	823	825	827	774	801
A_{1g}	577	583	610	612	566	615
E_u^3	505		494	500	469	498
E_g	447	448	445	447	429	472
B_{1u}^2	417		406	inactive	358	417
A_{2g}	406		inactive	inactive	424	413
E_u^2	388		inactive	388	354	393
A_{2u}	235	186	173	167	86.3*i*	191
E_u^1	201		189	183	124	144
B_{1u}^1	150		113	inactive	79	118
B_{1g}	113		142	143	154	132

is imaginary,[60] whereas SCC-DFTB and LDA-DFTB both predict that this mode is stable. Although SCC-DFTB is less accurate than LDA-DFT for the lowest frequency modes, the overall level of quantitative accuracy is impressive considering that the SCC-DFTB calculations are substantially faster than DFT.

In addition, we calculated an approximation to the infrared absorption spectrum using molecular dynamics (MD) simulations. The infrared absorption spectrum, $I(\omega)$, is proportional to the Fourier transform of the quantum mechanical electric dipole moment time-correlation function (TCF):[72,73]

$$I(\omega) \sim \int_{-\infty}^{\infty} dt\, e^{-i\omega t} \frac{\mathrm{Tr}[e^{-\beta\hat{H}}\hat{\mu}(0)\,\hat{\mu}(t)]}{\mathrm{Tr}[e^{-\beta\hat{H}}]} \qquad (10)$$

where $\hat{\mu}$ denotes the electric dipole moment operator of the system, $\hat{H}$ is the Hamiltonian operator for the nuclear and electronic degrees of freedom of the system, β is the inverse temperature times Boltzmann's constant ($\beta = 1/k_B T$), and Tr denotes a quantum mechanical trace over all degrees of freedom. Since eq 10 is generally computationally intractable, we utilized the classical dipole approximation[72−75] to replace the quantum mechanical electric dipole moment TCF by its classical analog

$$I(\omega) \sim Q(\omega) \int_{-\infty}^{\infty} dt\, e^{-i\omega t} \langle \mu(0)\mu(t) \rangle \qquad (11)$$

making it amenable to calculation within MD simulations. In eq 11 μ is the classical electric dipole moment of the system, the angular brackets represent a classical equilibrium ensemble average, and $Q(\omega)$ is a frequency dependent correction factor to compensate approximately for replacing a quantum mechanical TCF with a classical TCF.[76] In the present application, where we are primarily interested in peak locations of relatively low frequency vibrations (<850 cm^{-1}), we will assume $Q(\omega) = 1$. Since even computing the classical electric dipole TCF is nontrivial because it tends to be a slowly converging quantity, we instead invoked one further common approximation and calculated the Fourier transform of the velocity TCF

$$I_v(\omega) \sim \int_{-\infty}^{\infty} dt\, e^{-i\omega t} \langle v(0)v(t) \rangle \qquad (12)$$

where v is the $3N$-dimensional velocity vector. This last approximation has the disadvantage that the magnitude of the absorption intensity will not necessarily be accurate compared with experiment, but the location of the peaks in the spectrum should be maintained. For a further discussion of the approximations required to arrive at eq 12, see, for example, the discussion in the appendix of Lobaugh and Voth.[77] The advantage of eq 12 is that the phonon spectrum can readily be computed from MD simulations. In our MD simulations the system was first equilibrated for 1 ps in the NVT ensemble using an Andersen thermostat and for 1 ps without the theormostat.[78] The simulation then proceeded in the NVE ensemble, where the average temperature was observed to remain stable at the targeted temperature throughout the simulation. Production runs were between 20 and 50 ps with a time step of 1 fs. A slowly decaying exponential function was applied to the velocity TCF before it was Fourier transformed to force it smoothly to zero at long time. The spectra reported were completely insensitive to the details of this exponential function.

Figure 2 shows $I_v(\omega)$ at 30 and 300 K, where molecular dynamics has been performed on the six-atom unit cell. Restricting the size of the system to the primitive unit cell limits the spectrum to only reflect frequencies at the Γ point, thus ignoring dispersion effects. Temperature broadening of the peaks due to anharmonicity[74] is observed at 300 K. There is generally excellent agreement between the location of peaks in $I_v(\omega)$ compared to those computed with the dynamical matrix and/or frozen phonon methods. For example, the peak at 821 cm^{-1} corresponds to the highest frequency B_{2g} mode calculated as 822 and 823 cm^{-1} with the dynamical matrix and frozen phonon methods, respectively. Figure 3 shows $I_v(\omega)$ at 30 and 300 K, where MD has been performed on a $3 \times 3 \times 3$ supercell containing 162 atoms. The temperature broadening becomes more pronounced and more modes appear due to dispersion, as the supercell effectively includes more points in the Brillouin zone.

IV. TiO_2(110) Surface

A. Surface Geometry. The most stable termination of titania is the stoichiometric (110) surface, shown in Figure 4. The TiO_2(110) surface has a plane containing two titanium atoms (one 6-fold and one 5-fold coordinated) and two oxygen atoms per unit cell. One oxygen resides 1.3 Å above this plane (the bridging oxygen), and another oxygen sits similarly below the plane. These six atoms constitute the

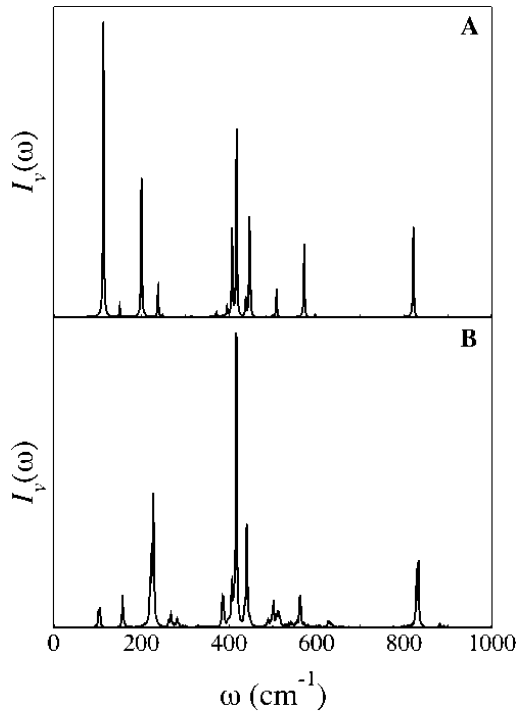

Figure 2. Phonon frequency spectrum, $I_\nu(\omega)$, calculated from the velocity time autocorrelation function, eq 12, at (A) 30 K and (B) 300 K for the six-atom rutile TiO_2 unit cell.

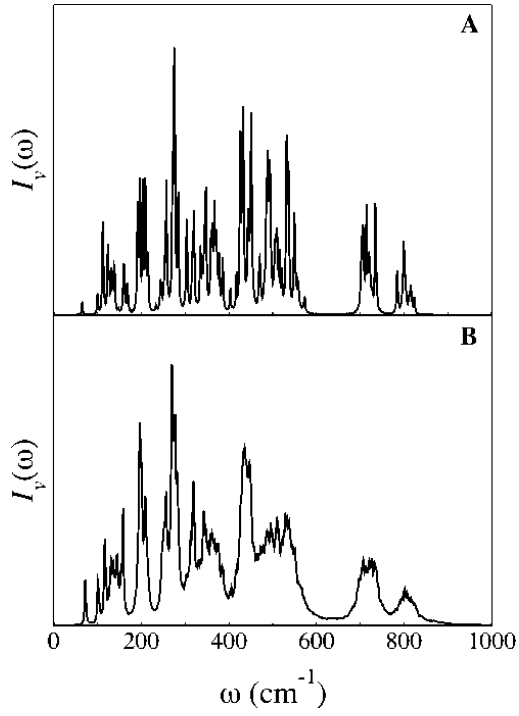

Figure 3. Phonon frequency spectrum, $I_\nu(\omega)$, calculated from the velocity time autocorrelation function, eq 12, at (A) 30 K and (B) 300 K for the a 162-atom 3 × 3 × 3 supercell of rutile TiO_2.

top layer, and lower layers are offset in the [$\bar{1}$10] direction by half a cell length. The first DFT studies of TiO_2(110) found that relaxations of the surface atoms from their bulk-terminated positions were substantial and responsible for a large reduction in calculated surface energies.[79,80] Many studies since have observed a strong dependence of relaxations and surface energy on slab thickness.[45,48,50,81] Figure 5 shows the convergence of the surface energy, $E_{surf} = (E_{slab} - E_{bulk})/2A$ (E_{slab} is the energy of the slab, E_{bulk} is the energy of an equivalent quantity of the bulk, and A is the surface area) with an increasing number of layers. It fluctuates about the converged value due to the structural difference between slabs with even and odd numbers of layers. Odd-layered slabs have a symmetry plane through the central layer, while this symmetry is absent in even-layered slabs. For sufficiently large slabs, these differences should cease to matter. The surface energy is reasonably well converged at seven layers, with a value of 0.116 eV/Å^2. Some recent DFT studies agree that the surface energy is approximately 0.056 eV/Å^2.[50,81] However, the exact value of E_{surf} depends strongly on the method and exchange-correlation functional used, dropping down to 0.030 eV/Å^2 with the PBE[54] functional.[82] Nevertheless, SCC-DFTB appears to overestimate the surface energy substantially.

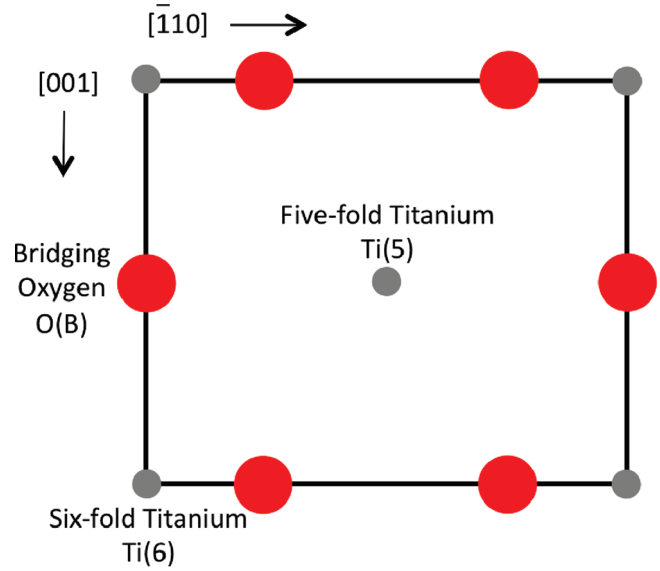

Figure 4. Schematic view of the idealized TiO_2(110) surface. Oxygen atoms are shown in red and titanium atoms in gray. All of the atoms are in the same plane, except for the bridging oxygens, O(B), which lie above the plane.

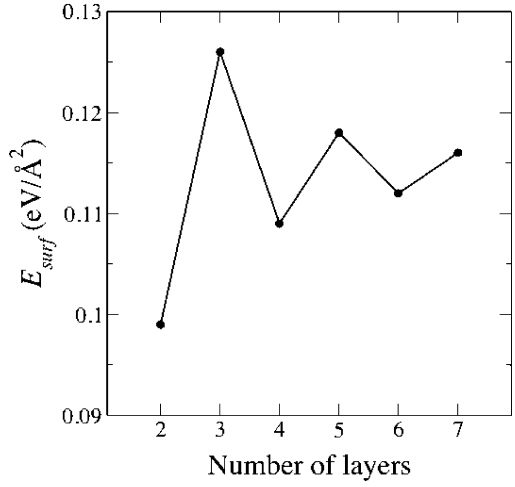

Figure 5. Convergence of the surface energy, E_{surf}, with the number of layers in the slab.

Table 3. Displacements of Surface Atoms, Perpendicular to the Surface, in Å as a Function of the Number of Layers in the Slab, *N*

	E_{surf} (eV/Å^2)	Ti(6)	Ti(5)	O(IP)	O(B)
$N = 4$	0.109	0.30	−0.22	0.14	0.07
$N = 5$	0.118	0.20	−0.16	0.16	−0.02
$N = 6$	0.112	0.28	−0.19	0.16	0.05
$N = 7$	0.116	0.23	−0.17	0.16	0.01
previous SCC-DFTB[30]		0.27	−0.11	0.22	0.07
PBE-DFT ($N = 8$)	0.029	0.35	−0.09	0.27	0.16
experiment[51]		0.25	−0.19	0.27	0.10

Table 4. Atomic Charges in Units of *e* of Surface and Internal Layer Atoms for the $N = 7$ TiO_2(110) Slab[a]

	Ti(6)	Ti(5)	O(IP)	O(B)	O(I)
surface layer	0.76	0.86	−0.40	−0.35	−0.45
middle layer	0.82	0.81	−0.41	−0.39	−0.39

[a] Charges in the bulk are 0.814*e* for Ti and −0.407*e* for O. O(I) corresponds to the subsurface oxygen directly under the bridging oxygen in the six-atom surface unit.

Table 3 lists the displacements of the surface atoms perpendicular to the surface. These atoms relax inward or outward from their bulk terminated positions, and the number of layers in the slab can greatly affect the size of these movements. A seven-layer slab, using SCC-DFTB, is reasonably well converged, and the displacements agree well with PBE-DFT calculations. Although some debate remains about the exact relaxations at the (110) surface,[83] the LEED results[51] shown in the Table 3 are representative and are well reproduced by our SCC-DFTB calculations. The atomic displacements normal to the surface are also consistent with the previous SCC-DFTB calculations (with different parameters) of Luschtinetz et al.[30] also shown in Table 3. Table 4 gives the atomic charges of the surface and middle layer atoms for the seven layer slab. Compared with the bulk, the 5-fold titanium has increased in charge, while the 6-fold titanium and bridging oxygen have decreased in charge. The charges on the middle layer agree with bulk charges to within 0.02*e*, confirming that the slab is large enough for the interior to behave like the bulk material.

B. TiO_2(110) Electronic Structure. Previous studies have widely agreed that no surface electronic states are observed or predicted for TiO_2(110).[44] Figure 6 shows the electronic density of states for a four-layer slab of TiO_2(110) containing 24 atoms calculated with SCC-DFTB, compared to that of the bulk. The band structure was obtained by self-consistently converging charges with a tolerance of 1×10^{-5} on a $2 \times 4 \times 1$ Monkhorst−Pack mesh[61] in **k**-space. These charges were then utilized in a non-self-consistent-charge calculation of the energy along the high symmetry directions of the Brillouin zone. As expected, the presence of the stoichiometric surfaces in the supercell does not have an appreciable effect on the electronic structure; the valence and lower conduction bands have a similar number of peaks in terms of location and magnitude as the bulk, and the direct band gap of 2.46 eV is maintained. The gap between the t_{2g} and e_g conduction bands at around 5 eV shows the largest difference, decreasing from a gap of approximately 1 eV to less than 0.5 eV.

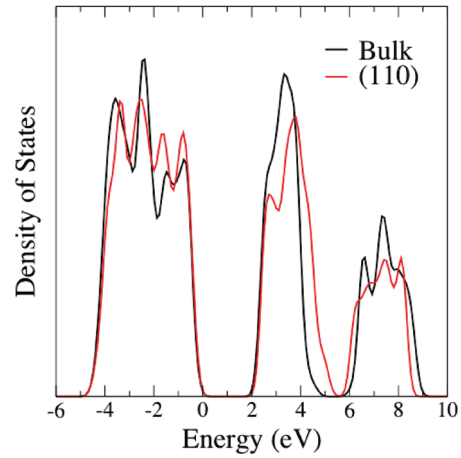

Figure 6. Comparison of the electronic density of states between bulk TiO_2 and a slab of TiO_2(110). The number of atoms in both systems is 24. The zero is taken as the Fermi energy of the bulk system.

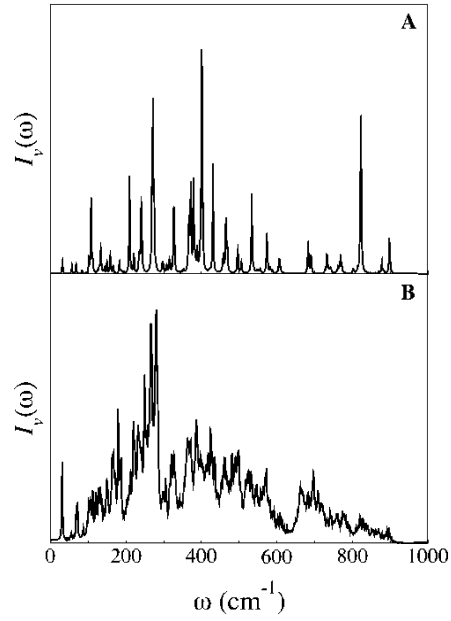

Figure 7. Phonon frequency spectra, $I_v(\omega)$, calculated from the velocity time autocorrelation function, eq 12. (A) 30 K with a TiO_2 (110) slab containing 24 atoms and (B) 300 K with a TiO_2(110) slab containing 96 atoms.

C. TiO_2(110) Vibrational Spectra. Two experimental measurements of the (110) phonon spectrum have appeared in the literature using electron energy loss spectroscopy (EELS)[84] and high-resolution EELS (HREELS).[85] The HREELS study found three bands at approximately 365, 445, and 755 cm^{-1}, which were consistent with the earlier EELS measurements. Figure 7 shows the phonon frequency spectrum, $I_v(\omega)$, calculated as the Fourier transform of the velocity TCF (eq 12) of (A) a 30 ps NVE MD simulation TiO_2 (110) slab containing 24 atoms equilibrated to 30 K and (B) a 20 ps MD simulation of a TiO_2(110) slab containing 96 atoms at 300 K. The spectra retain some of the features of the bulk phonon spectra (Figures 2 and 3), particularly the characteristic gap around 640 cm^{-1}. A direct comparison of the calculated spectra to experiment is not possible without a detailed model for intensities of the surface modes as measured with HREELS. We also performed

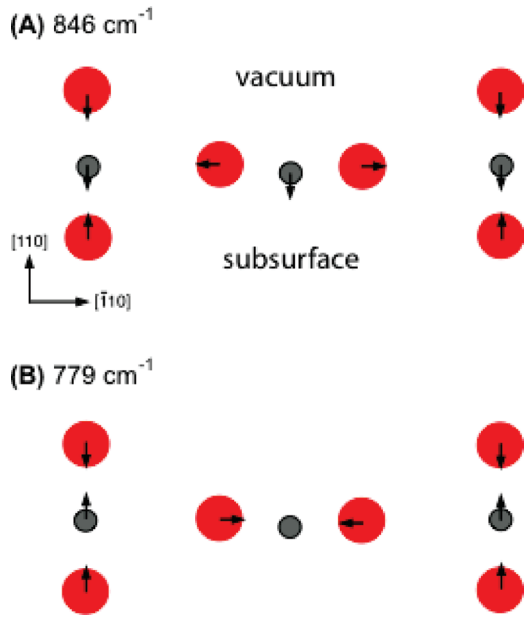

Figure 8. Schematic illustration of two surface vibration modes found using the dynamical matrix method for TiO_2(110). The view is perpendicular to the plane of the surface, and oxygen atoms are shown in red and titanium atoms in gray.

a dynamical matrix calculation on a subset of a 24-atom slab of TiO_2(110), corresponding to the six atoms of one surface. The two highest frequency modes (846 and 779 cm^{-1}) involve motions of the bridging oxygen, 6-fold coordinated titanium, and a subsurface oxygen perpendicular to the plane of the (110) surface, as well as motions of the in-plane oxygen atoms parallel to the surface (Figure 8). Another mode of interest involves the opposite motion of the in-plane oxygens and 5-fold Ti atoms (428 cm^{-1}).

V. Conclusions

SCC-DFTB is a computationally efficient semiempirical tight-binding method, which has been successfully applied to crystals and crystal surfaces, as well as biological systems. Because it is relatively inexpensive compared with conventional DFT methods, it is possible to simulate systems containing large numbers of atoms or to perform long molecular dynamics simulations. Titanium dioxide has been extensively studied by DFT, but cell sizes have mostly been limited to contain under 100 atoms, and molecular dynamics run lengths are restricted to a few tens of picoseconds. DFTB+ molecular dynamics simulations based on SCC-DFTB forces are hundreds of times faster than equivalent VASP calculations based on DFT forces. Although SCC-DFTB parameters have not yet been parametrized specifically for titania, we have demonstrated that existing parameters for titanium in biological systems reproduce properties of the material well. A band gap of 2.46 eV is predicted, closer to experiment than DFT results. Other electronic properties and vibrational mode frequencies also agree well with experiment and theory. Relaxations of (110) surface atoms are well-reproduced, and although the surface energy is overestimated by perhaps a factor of 2, this property has been seen to be strongly method-dependent and is therefore not necessarily of large concern. On the basis of these encouraging results, computationally efficient investigations of more complex phenomena involving the TiO_2 surface (e.g., reactions of adsorbate molecules) with SCC-DFTB are justified and are presently being pursued.

Acknowledgment. The authors are grateful for support from the University of Notre Dame Energy Center and the University of Notre Dame Center for Research Computing.

References

(1) Seifert, G. *J. Phys. Chem. A* **2007**, *111*, 5609.

(2) Seifert, G.; Porezag, D.; Frauenheim, T. *Int. J. Quantum Chem.* **1996**, *58*, 185.

(3) Elstner, M.; Porezag, D.; Jungnickel, G.; Elsner, J.; Haugk, M.; Frauenheim, T.; Suhai, S.; Seifert, G. *Phys. Rev. B* **1998**, *58*, 7260.

(4) Porezag, D.; Frauenheim, T.; Kohler, T.; Seifert, G.; Kaschner, R. *Phys. Rev. B* **1995**, *51*, 12947.

(5) Frauenheim, T.; Seifert, G.; Elstner, M.; Niehaus, T.; Kohler, C.; Amkreutz, M.; Sternberg, M.; Hajnal, Z.; Di Carlo, A.; Suhai, S. *J. Phys.-Condens. Mat.* **2002**, *14*, 3015.

(6) Moreira, N. H.; Dolgonos, G.; Aradi, B.; da Rosa, A. L.; Frauenheim, T. *J. Chem. Theory Comput.* **2009**, *5*, 605.

(7) Rauls, E.; Elsner, J.; Gutierrez, R.; Frauenheim, T. *Solid State Commun.* **1999**, *111*, 459.

(8) Kohler, C.; Frauenheim, T. *Surf. Sci.* **2006**, *600*, 453.

(9) Lin, C. S.; Zhang, R. Q.; Lee, S. T.; Elstner, M.; Frauenheim, T.; Wan, L. J. *J. Phys. Chem. B* **2005**, *109*, 14183.

(10) Elstner, M. *Theor. Chem. Acc.* **2006**, *116*, 316.

(11) Elstner, M.; Frauenheim, T.; Kaxiras, E.; Seifert, G.; Suhai, S. *Phys. Status Solidi B* **2000**, *217*, 357.

(12) Elstner, M.; Jalkanen, K. J.; Knapp-Mohammady, M.; Frauenheim, T.; Suhai, S. *Chem. Phys.* **2000**, *256*, 15.

(13) Elstner, M.; Jalkanen, K. J.; Knapp-Mohammady, M.; Frauenheim, T.; Suhai, S. *Chem. Phys.* **2001**, *263*, 203.

(14) Hu, H.; Elstner, M.; Hermans, J. *Proteins* **2003**, *50*, 451.

(15) Jalkanen, K. J.; Elstner, M.; Suhai, S. *J. Mol. Struct. THEOCHEM* **2004**, *675*, 61.

(16) Kumar, A.; Elstner, M.; Suhai, S. *Int. J. Quantum Chem.* **2003**, *95*, 44.

(17) Kumar, A.; Knapp-Mohammady, M.; Mishra, P. C.; Suhai, S. *J. Comput. Chem.* **2004**, *25*, 1047.

(18) Liu, H. Y.; Elstner, M.; Kaxiras, E.; Frauenheim, T.; Hermans, J.; Yang, W. T. *Proteins* **2001**, *44*, 484.

(19) Okada, T.; Sugihara, M.; Bondar, A. N.; Elstner, M.; Entel, P.; Buss, V. *J. Mol. Biol.* **2004**, *342*, 571.

(20) Reha, D.; Kabelac, M.; Ryjacek, F.; Sponer, J.; Sponer, J. E.; Elstner, M.; Suhai, S.; Hobza, P. *J. Am. Chem. Soc.* **2002**, *124*, 3366.

(21) Shishkin, O. V.; Elstner, M.; Frauenheim, T.; Suhai, S. *Int. J. Mol. Sci.* **2003**, *4*, 537.

(22) Shishkin, O. V.; Gorb, L.; Luzanov, A. V.; Elstner, M.; Suhai, S.; Leszczynski, J. *J. Mol. Struct. THEOCHEM* **2003**, *625*, 295.

(23) Sugihara, M.; Buss, V.; Entel, P.; Elstner, M.; Frauenheim, T. *Biochemistry* **2002**, *41*, 15259.

(24) Wanko, M.; Hoffmann, M.; Strodel, P.; Koslowski, A.; Thiel, W.; Neese, F.; Frauenheim, T.; Elstner, M. *J. Phys. Chem. B* **2005**, *109*, 3606.

(25) Zhou, H. Y.; Tajkhorshid, E.; Frauenheim, T.; Suhai, S.; Elstner, M. *Chem. Phys.* **2002**, *277*, 91.

(26) Yu, H. B.; Cui, Q. *J. Chem. Phys.* **2007**, *127*, 234504.

(27) Hu, H.; Lu, Z. Y.; Elstner, M.; Hermans, J.; Yang, W. T. *J. Phys. Chem. A* **2007**, *111*, 5685.

(28) Enyashin, A. N.; Ivanovskii, A. L. *J. Mol. Struct. THEOCHEM* **2006**, *766*, 15.

(29) Enyashin, A. N.; Seifert, G. *Phys. Status Solidi B* **2005**, *242*, 1361.

(30) Luschtinetz, R.; Frenzel, J.; Milek, T.; Seifert, G. *J. Phys. Chem. C* **2009**, *113*, 5730.

(31) http://www.dftb.org.

(32) Zheng, G.; Witek, H. A.; Bobadova-Parvanova, P.; Irle, S.; Musaev, G.; Prabhakar, R.; Morokuma, K.; Lundberg, M.; Elstner, M.; Kohler, C.; Frauenheim, T. *J. Chem. Theory Comput.* **2007**, *3*, 1349.

(33) Fox, M. A.; Dulay, M. T. *Chem. Rev.* **1993**, *93*, 341.

(34) Fujishima, A.; Honda, K. *Nature* **1972**, *238*, 37.

(35) Fujishima, A.; Rao, T. N.; Tryk, D. A. *J. Photochem. Photobiol. C* **2000**, *1*, 1.

(36) Harada, H.; Ueda, T. *Nouv. J. Chim.* **1984**, *8*, 123.

(37) Hoffmann, M. R.; Martin, S. T.; Choi, W. Y.; Bahnemann, D. W. *Chem. Rev.* **1995**, *95*, 69.

(38) Kamat, P. V. *Chem. Rev.* **1993**, *93*, 267.

(39) Kawai, M.; Naito, S.; Tamaru, K.; Kawai, T. *Chem. Phys. Lett.* **1983**, *98*, 377.

(40) Kawai, T.; Sakata, T. *J. Chem. Soc. Chem. Commun.* **1980**, 694.

(41) Linsebigler, A. L.; Lu, G. Q.; Yates, J. T. *Chem. Rev.* **1995**, *95*, 735.

(42) Sakata, T. *J. Photochem.* **1985**, *29*, 205.

(43) Sakata, T.; Kawai, T. *Chem. Phys. Lett.* **1981**, *80*, 341.

(44) Diebold, U. *Surf. Sci. Rep.* **2003**, *48*, 53.

(45) Bates, S. P.; Kresse, G.; Gillan, M. J. *Surf. Sci.* **1997**, *385*, 386.

(46) Harrison, N. M.; Wang, X. G.; Muscat, J.; Scheffler, M. *Faraday Discuss.* **1999**, *114*, 305.

(47) Lindan, P. J. D.; Harrison, N. M.; Gillan, M. J.; White, J. A. *Phys. Rev. B* **1997**, *55*, 15919.

(48) Bredow, T.; Giordano, L.; Cinquini, F.; Pacchioni, G. *Phys. Rev. B* **2004**, *70*, 035419.

(49) Muscat, J.; Harrison, N. M.; Thornton, G. *Phys. Rev. B* **1999**, *59*, 2320.

(50) Swamy, V.; Muscat, J.; Gale, J. D.; Harrison, N. M. *Surf. Sci.* **2002**, *504*, 115.

(51) Lindsay, R.; Wander, A.; Ernst, A.; Montanari, B.; Thornton, G.; Harrison, N. M. *Phys. Rev. Lett.* **2005**, *94*, 246102.

(52) Charlton, G.; Howes, P. B.; Nicklin, C. L.; Steadman, P.; Taylor, J. S. G.; Muryn, C. A.; Harte, S. P.; Mercer, J.; McGrath, R.; Norman, D.; Turner, T. S.; Thornton, G. *Phys. Rev. Lett.* **1997**, *78*, 495.

(53) Perdew, J. P.; Zunger, A. *Phys. Rev. B* **1981**, *23*, 5048.

(54) Perdew, J. P.; Burke, K.; Ernzerhof, M. *Phys. Rev. Lett.* **1996**, *77*, 3865.

(55) Perdew, J. P.; Wang, Y. *Phys. Rev. B* **1992**, *45*, 13244.

(56) Foulkes, W. M. C.; Haydock, R. *Phys. Rev. B* **1989**, *39*, 12520.

(57) Riccardi, D.; Schaefer, P.; Yang, Y.; Yu, H. B.; Ghosh, N.; Prat-Resina, X.; Konig, P.; Li, G. H.; Xu, D. G.; Guo, H.; Elstner, M.; Cui, Q. *J. Phys. Chem. B* **2006**, *110*, 6458.

(58) Aradi, B.; Hourahine, B.; Frauenheim, T. *J. Phys. Chem. A* **2007**, *111*, 5678.

(59) Burdett, J. K.; Hughbanks, T.; Miller, G. J.; Richardson, J. W.; Smith, J. V. *J. Am. Chem. Soc.* **1987**, *109*, 3639.

(60) Montanari, B.; Harrison, N. M. *Chem. Phys. Lett.* **2002**, *364*, 528.

(61) Monkhorst, H. J.; Pack, J. D. *Phys. Rev. B* **1976**, *13*, 5188.

(62) Glassford, K. M.; Chelikowsky, J. R. *Phys. Rev. B* **1992**, *46*, 1284.

(63) Labat, F.; Baranek, P.; Domain, C.; Minot, C.; Adamo, C. *J. Chem. Phys.* **2007**, *126*, 154703.

(64) Kowalczyk, S. P.; McFeely, F. R.; Ley, L.; Gritsyna, V. T.; Shirley, D. A. *Solid State Commun.* **1977**, *23*, 161.

(65) Pascual, J.; Camassel, J.; Mathieu, H. *Phys. Rev. B* **1978**, *18*, 5606.

(66) Vos, K. *J. Phys. C Solid State* **1977**, *10*, 3917.

(67) Trayler, J. G.; Smith, H. G.; Nicklow, R. M.; Wilkinso, Mk. *Phys. Rev. B* **1971**, *3*, 3457.

(68) Porto, S. P. S.; Fleury, P. A.; Damen, T. C. *Phys. Rev.* **1967**, *154*, 522.

(69) Eagles, D. M. *J. Phys. Chem. Solids* **1964**, *25*, 1243.

(70) Sikora, R. *J. Phys. Chem. Solids* **2005**, *66*, 1069.

(71) Lee, C.; Ghosez, P.; Gonze, X. *Phys. Rev. B* **1994**, *50*, 13379.

(72) Gordon, R. G. *J. Chem. Phys.* **1965**, *43*, 1307.

(73) McQuarrie, D. A. *Statistical Mechanics*; University Science Books: Sausalito, CA, 2000.

(74) Schmidt, J. R.; Corcelli, S. A. *J. Chem. Phys.* **2008**, *128*, 184504.

(75) Berens, P. H.; Wilson, K. R. *J. Chem. Phys.* **1981**, *74*, 4872.

(76) Egorov, S. A.; Everitt, K. F.; Skinner, J. L. *J. Phys. Chem. A* **1999**, *103*, 9494.

(77) Lobaugh, J.; Voth, G. A. *J. Chem. Phys.* **1997**, *106*, 2400.

(78) Andersen, H. C. *J. Chem. Phys.* **1980**, *72*, 2384.

(79) Ramamoorthy, M.; Kingsmith, R. D.; Vanderbilt, D. *Phys. Rev. B* **1994**, *49*, 7709.

(80) Ramamoorthy, M.; Vanderbilt, D.; Kingsmith, R. D. *Phys. Rev. B* **1994**, *49*, 16721.

(81) Hameeuw, K. J.; Cantele, G.; Ninno, D.; Trani, F.; Iadonisi, G. *J. Chem. Phys.* **2006**, *124*, 024708.

(82) Kiejna, A.; Pabisiak, T.; Gao, S. W. *J. Phys.-Condens. Mat.* **2006**, *18*, 4207.

(83) Pang, C. L.; Lindsay, R.; Thorton, G. *Chem. Soc. Rev.* **2008**, *37*, 2328.

(84) Rocker, G.; Schaefer, J. A.; Gopel, W. *Phys. Rev. B* **1984**, *30*, 3704.

(85) Henderson, M. A. *Surf. Sci.* **1996**, *355*, 151.

(86) Knotek, M. L.; Feibelman, P. J. *Phys. Rev. Lett.* **1978**, *40*, 964.

CT900665A